Two- and Three-Dimensional Au Nanoparticle/CoTMPyP Self-Assembled Nanotructured Materials: Film Structure, Tunable Electrocatalytic Activity, and Plasmonic Properties

Wenlong Cheng,[†,‡] Shaojun Dong,[*,†] and Erkang Wang[*,†]

State Key Laboratory of Electroanalytical Chemistry, Changchun Institute of Applied Chemistry, Chinese Academy of Sciences, Changchun, Jilin, 130022, People's Republic of China, and Graduate School of the Chinese Academy of Sciences, Beijing, 100039, People's Republic of China

Received: July 28, 2004; In Final Form: September 30, 2004

Two- and three-dimensional Au nanoparticle/[tetrakis(*N*-methylpyridyl)porphyrinato]cobalt (CoTMPyP) nanostructured materials were prepared by "bottom-up" self-assembly. The electrocatalytic and plasmonic properties of the Au nanoparticle/CoTMPyP self-assembled nanostructured materials (abbreviated as Au/CoTMPyP SANMs) are tunable by controlled self-assembly of the Au nanoparticles and CoTMPyP on indium tin oxide (ITO) electrode. The electrocatalytic activity of the Au/CoTMPyP SANMs can be tuned in two ways. One way is that citrate-stabilized Au nanoparticles are positioned first on ITO surface with tunable number density, and then positively charged CoTMPyP ions are planted selectively on these gold sites. The other way is that Au nanoparticles and CoTMPyP are deposited by virtue of layer-by-layer assembly, which can also tune the amount of the as-deposited electrocatalysts. FE-SEM studies showed that three-dimensional SANMs grow in the lateral expansion mode, and thermal annealing resulted in both surface diffusion of nanoparticles and atomic rearrangement to generate larger gold nanostructures with predominant (111) facets. The annealed SANMs show a strongly enhancing gold surface plasmonic resonance band in comparison with unannealed SANMs. The changes in gold plasmonic properties correlate with annealing-induced structural changes of the SANMs.

Introduction

Metallic nanoparticles exhibit interesting optical, electric, magnetic, and catalytic properties different from their corresponding bulk materials, and these unique properties are tunable by particle size,[1] shape,[2] surface chemistry,[3] and surrounding nanoenvironments.[3f,4] Potential utilization of these nanoscale building blocks in future nanodevices still needs development of versatile approaches to assemble or integrate nanoparticles into desired nanostructures; therefore, considerable research effort is now being directed toward self-assembly of metallic nanoparticles into two-dimensional (2D) or three-dimensional (3D) nanoarchitectures. Two-dimensional nanoparticle arrays that can be fabricated physically[5] or chemically[6] show unusual optical properties strikingly different from these of bulk metal.[7] Compared with physical strategy[5] for the 2D arrays, wet chemical approaches[6] provide easier control over island size and shape by nanoparticle synthesis chemistry and also require no expensive apparatus.[6] In addition, it has been shown that the metallic island arrays fabricated by the wet chemical strategy exhibit potential applications in surface-enhanced Raman spectroscopy (SERS) and surface plasmon resonance (SPR),[6a,b,8] and also can be used as substrates for electrochemical studies.[9]

Three-dimensional nanoparticle arrays can be fabricated simply by layer-by-layer (LBL) assembly, which was initially developed by G. Decher to deposit charged polyelectrolyte pairs on a solid support. Multilayers of charged nanoparticles were usually fabricated by virtue of oppositely charged polyelectrolytes in a cyclic adsorption manner.[10] Three-dimensional nanoparticle arrays can also be fabricated by virtue of molecular cross-linker in a way analogous to the construction of nanoparticle/polymer LBL films. The driving force for molecularly linked nanoparticle multilayers can be electrostatic attraction, covalent bonding, or both. Willner et al. have made use of several kinds of oligocations as cross-linkers and fabricated successfully 3D Au nanoparticle arrays by electrostatic interactions.[11] The 3D nanoparticle arrays are optically and electrically accessible, showing potential applications in photoelectrochemistry,[12] electronics,[13] and sensing.[14] Interestingly, the 3D nanoparticle arrays are porous, and even molecular recognition units and biomolecules can be incorporated into the arrays to result in electrochemically accessible responses.[11−15] The bisthiol molecule can also cross-link gold nanoparticles into 3D arrays by covalent interactions,[16] and it binds covalently to nanoparticle surfaces with one thiol end and leaves another thiol end exposed upon immersion of primary nanoparticle layer into bisthiol solution. Further treatment with the colloid leads to additional adsorption of nanoparticles on the thiol layer; thus, 3D arrays can be fabricated in a cyclic manner. The functional units such as electroactive viologen can be incorporated into the multilayers by molecular design.[17] Three-dimensional nanoparticle arrays can also be constructed by mixed electrostatic and covalent interactions.[9e,18]

In fact, 2D and 3D nanoparticle arrays represent a unique class of materials, whose optoelectric properties are highly tunable by controlled self-assembly. For example, LBL can produce stratified films with alternating layers of organic and inorganic substances without phase segregation.[19] Compared with films from other film-fabricating methods,[20] 2D and 3D nanoparticle-based self-assembled nanostructured materials

* Corresponding author. Fax: +86-431-5689711. E-mail: ekwang@ciac.jl.cn.

† Changchun Institute of Applied Chemistry, Chinese Academy of Sciences.

‡ Graduate School of the Chinese Academy of Sciences.

10.1021/jp0466237 CCC: $27.50
Published on Web 11/17/2004

(SANMs) can be generated on substrate with various shapes,[10c,21,22] and the accuracy of the thin film deposition is improved significantly. The resulting films can be conductive, semiconductive, or insulative depending on the thickness of cross-linker layers.[23]

Herein, we prepared 2D and 3D Au/CoTMPyP SANMs by a "bottum-up" self-assembly strategy. The as-fabricated 2D or 3D Au nanoparticle/CoTMPyP assemblies are a novel class of materials, whose plasmonic and electrocatalytic properties are highly controllable by self-assembly. We identified several novel properties and structural nature of the Au/CoTMPyP SANMs: (1) Deposition of CoTMPyP is highly selective to nano-gold sites; as a result, a tunable electrocatalytic activity toward dioxygen reduction is achieved in 2D space parellel to the electrode surface. (2) The quantity of immobilized CoTMPyP is also tunable by LBL assembly, which modulates electrocatalytic activity toward dioxygen reduction in 3D space above the electrode surface. (3) Three-dimensional SANMs grow in the lateral expansion mode. (4) The as-prepared 3D SANMs are made of "huge" mountains and "vast" plains, where the former consist of piled nanoparticles and the latter are made of many small in-plane nanoparticle aggregates and discrete nanoparticles. (5) Annealing leads to atomic rearrangement in both 2D and 3D SANMs to generate more gold(111) facets. Simultaneously, the localized gold surface plasmon resonance was found to enhance dramatically after annealing. These properties correlate with the structure of the nanostructured materials.

Experimental Section

Reagents. $HAuCl_4 \cdot 3H_2O$, trisodium citrate, and (3-aminopropyl)trimethoxysilane (APTMS) were obtained from Aldrich and used as received. $CoTMPyP(ClO_4)_5$ was synthesized according to the literature[24] and has been used as a counterion in our previous LBL studies.[25] All other reagents were of analytical grade and were used also without further purification. Pure water was obtained by passing it through a Millipore Milli-Q water purification system. Its resistivity is over 18 MΩ·cm. Indium doped tin oxide (ITO) glass was purchased from Changchun Institute of Optics and Mechanics with a square resistance of 80 $\Omega \cdot cm^{-2}$.

Instrumentation. The UV−visible spectra were acquired using a Cary 500 UV−visible NTR spectrometer (Varian, USA). Electrochemical experiments were carried out on an Autolab PGSTAT30 potentiostat (Utrecht, The Netherlands) in a conventional one-compartment cell. The cell was housed in a homemade Faraday cage to reduce stray electrical noise. All measurements were done using standard three-electrode systems. A Ag/AgCl electrode was used as the reference electrode, a Pt foil was used as the counter electrode, and an O-ring with a 6 mm inner diameter was used to seal the ITO electrode for all electrochemical experiments (geometry area was ca. 0.283 cm^2). Photographs were taken by a FinePixViewer 6900 camera made by Fuji Photo Film Co., Ltd. The conductive ITO film with attached gold nanoparticles was imaged by an XL30 ESEM FEG field emission scanning electron microscopy (FEI Company). X-ray diffraction (XRD) analysis of glass-supported nanoparticle films was carried out on a Rigaku D/Max 2500 V/PC X-ray diffractometer (made in Japan) using Cu (50 kV, 250 mA) radiation.

Preparation of the SANMs. The Au nanoparticles used in this study were prepared by the conventional citrate reduction of $HAuCl_4$ in water at near-boiling temperature as described previously.[1a,6,8,9,11−14] ITO glass slides with 1.0 cm × 1.0 cm dimensions were sonicated for 20 min in each of the following solvents: soapy water, water, acetone, and methanol. After thorough cleaning, the ITO slides were immersed in 2% (v:v) APTMS methanol solution for 1 day. After exhaustive rinsing by methanol, five APTMS-modified ITO slides were then immersed in the as-prepared Au colloid (∼6 nM) for 10, 20, 32, 95, and 180 min, respectively. After thorough rinsing with water, the five slides were immersed in 0.3 mM CoTMPyP solution for 30 min before electrochemical scanning in air-saturated 0.1 M $HClO_4$ aqueous solution. Thus, 2D SANMs were fabricated in a highly controllable way by a time-tuning self-assembly.

Three-dimensional SANMs were built up by sequential immersion of the ITO slide with Au nanoparticle monolayer into 0.3 mM CoTMPyP aqueous solution for 20 min and the as-prepared Au colloid for 60 min. The above two steps were repeated alternately until the desired number of layers was reached. The conductive sides of two ITO slides with one Au nanoparticle layer and with seven Au nanoparticle layers were imaged directly by field emission scanning electron microscopy (FE-SEM), and the conductive sides were connected to the base copper substrates by a conductive adhesive tape to decrease sample charging. The two ITO slides with one Au nanoparticle layer and with seven Au nanoparticle layers were annealed by placing them in an oven at 600 °C for 5 h; they were cooled to room temperature, and then the conductive surfaces with nanoparticle films were imaged directly without any metallic coating following the aforementioned method.

Results and Discussion

Two-Dimensional Au/CoTMPyP SANMs: Site Selectivity and Two-Dimensionally Tunable Electrocatalytic Activities toward Dioxygen Reduction. The 2D SANMs was prepared by a wet chemical self-assembly strategy. In the first step, well-controlled 2D Au nanoparticle arrays with a tunable particle number per unit area were fabricated.[6,26] In the second step, CoTMPyP was planted selectively on these nano-gold sites to create Au nanoparticle/CoTMPyP nanocomposites. The site-selective binding of CoTMPyP on nano-gold sites generates discrete nanosized Au nanoparticle/CoTMPyP units. The nanosized units distributed evenly on the 2D ITO surface, and the ensembles of the discrete units are so-called 2D SANMs.

ITO-supported 2D gold nanoparticle arrays are robust and can survive various solvent rinsings and electrochemical scanning in the potential range of 0−1.5V.[6,8,9] Further molecular modification on the arrays usually does not result in particle desorption as demonstrated by previous works.[9] By virtue of such "preimmobilization and then modification" strategy, molecular monolayer,[9a] bilayer,[9b] multilayer,[9c] atomic monolayer,[9d,e] and polymer[9f] were successfully positioned onto nanoparticle surfaces to generate 2D gold/organic nanostructured materials. Actually, this strategy is advantageous over direct modification on solution-state nanoparticles, the aggregation of nanoparticles can be avoided, and the resulting assemblies are accessible to direct electrochemical and optical investigation. These nano-surface-supported molecular self-assembly systems show interesting electrochemical[9a−d] and chemical properties[9f] different from bulk surface-supported corresponding systems. However, these previous studies do not report the tunability of electrocatalytic properties of nanostructured materials prepared by the above strategy. Here, CoTMPyP was selected as a binding molecule due to its high electrochemical activity toward dioxygen reduction.[25] The electrocatalytic currents are highly sensitive to subtle changes in the number density of Au nanoparticles. As a result, 2D tunable electrocatalytic activity was achieved by controlled preparation of 2D SANMs.

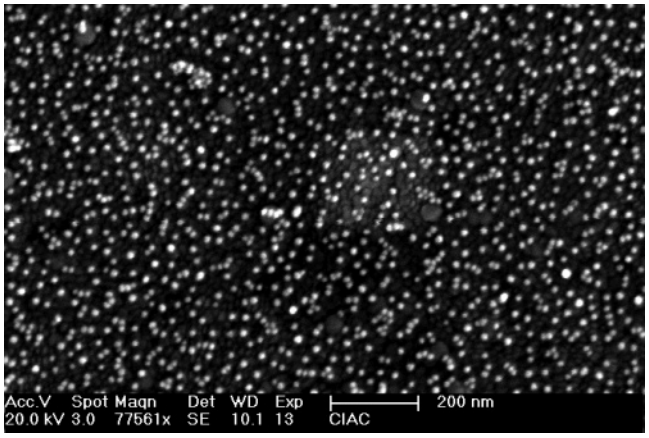

Figure 1. Typical FE-SEM micrograph of as-prepared 2D Au nanoparticle array supported on ITO.

A 2D Au nanoparticle array was fabricated using (3-aminopropyl)trimethoxysilane (APTMS) as a polymeric adhesive layer for presynthesized gold nanoparticles, which has been described previously.[6,8−9] Figure 1 shows a typical FE-SEM image of the as-prepared 2D Au nanoparticle array. The bright features correspond to gold nanoparticles, which are uniformly distributed on ITO substrate. It has to be noted that the APTMS layer is positively charged (with amino group exposed) and would not favor CoTMPyP binding on it, whereas the as-anchored Au nanoparticles are still negatively charged. CoTMPyP would prefer to locate on nano-gold sites. That is, CoTMPyP deposition should be site-specific to nano-gold sites, which was supported experimentally by following UV−visible absorbance spectroscopy. The notable sensitivity of surface plasmon resonance spectroscopy to the presence of absorbents provides an effective route for monitoring CoTMPyP binding to gold nanoparticles.[5,9,27−29] The localized refractive index surrounding gold nanoparticels would change upon molecular binding, which would result in an absorbance increase and red shift of native gold surface plasmon band. Figure 2 shows absolute spectra and difference spectra of CoTMPyP on the 2D Au nanoparticle array, demonstrating clearly a site-selective deposition property to nano-gold sites. The anchoring of CoTMPyP on gold nanoparticles was supported by the concurrent appearance of CoTMPyP Soret band and an increase and red shift (from 521 to 526 nm) of gold surface plasmon absorption in the absolute spectra (Figure 2A). The difference spectra (Figure 2B) give clearer evidence of CoTMPyP binding to gold nanoparticles. In contrast, the CoTMPyP-treated APTMS/ITO showed no clear Soret band in both absolute and difference spectra, indicative of little absorption of CoTMPyP on APTMS. The negative peak in Figure 2B might result from the desorption of loosely bound APTMS or contamination after immersion into CoTMPyP solution.

It has been known that CoTMPyP is an efficient electrocatalyst toward dioxygen reduction following usually a two-electron process.[25] The CoTMPyP-treated APTMS/ITO shows negligible electrocatalytic current (curve 2 in the top part of Figure 3), demonstrating little adsorption of CoTMPyP on ITO. Thus, site-selective deposition of CoTMPyP on nano-gold sites was also supported by electrochemistry. Comparison of curve 1 with curve 3 in Figure 3 shows clearly that gold nanoparticles play also a role in catalyzed reduction of dioxygen. Further attachment of CoTMPyP enhances catalytic activity, as demonstrated by increasing the peak current and positive shift in peak potential (curve 4). As for irreversible reductive reactions, the number of electrons transferred can be roughly estimated according to the $i \sim V$ equation,[30] from which the number of electrons transferred for the dioxygen reduction can be determined. As a result, the number of electrons transferred was estimated as ~2,

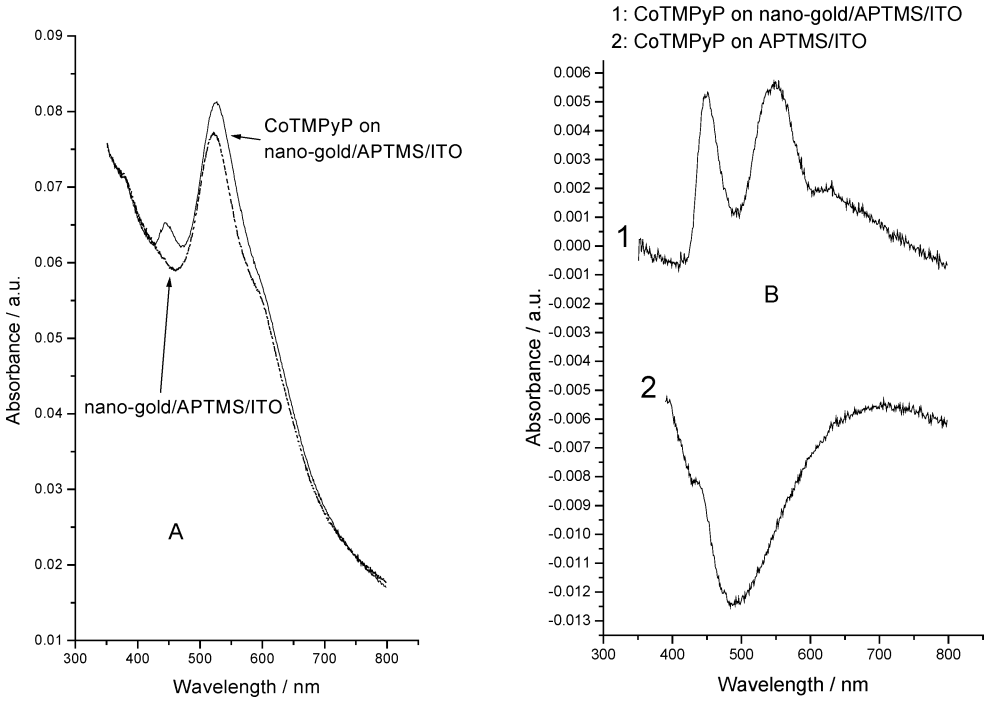

Figure 2. UV−visible spectroscopy monitoring for site-selective deposition of CoTMPyP on 2D Au nanoparticle array. (A) Absolute spectra of nano-gold/APTMS/ITO before (dashed line) and after (solid line) immersion into 0.3 mM CoTMPyP aqueous solution for 30 min. (B) Difference spectra obtained by subtraction of before-immersion spectra from after-immersion spectra into CoTMPyP. CoTMPyP-treated nano-gold/APTMS/ITO results in simultaneous appearance of characteristic Soret band of CoTMPyP at ~449 nm and enhanced surface plasmon band at ~548 nm, demonstrating an efficient immobilization of CoTMPyP on nano-gold sites. In contrast, CoTMPyP-treated APTMS/ITO (curve 2) shows no obvious Soret band, demonstrating little adsorption of CoTMPyP on APTMS films.

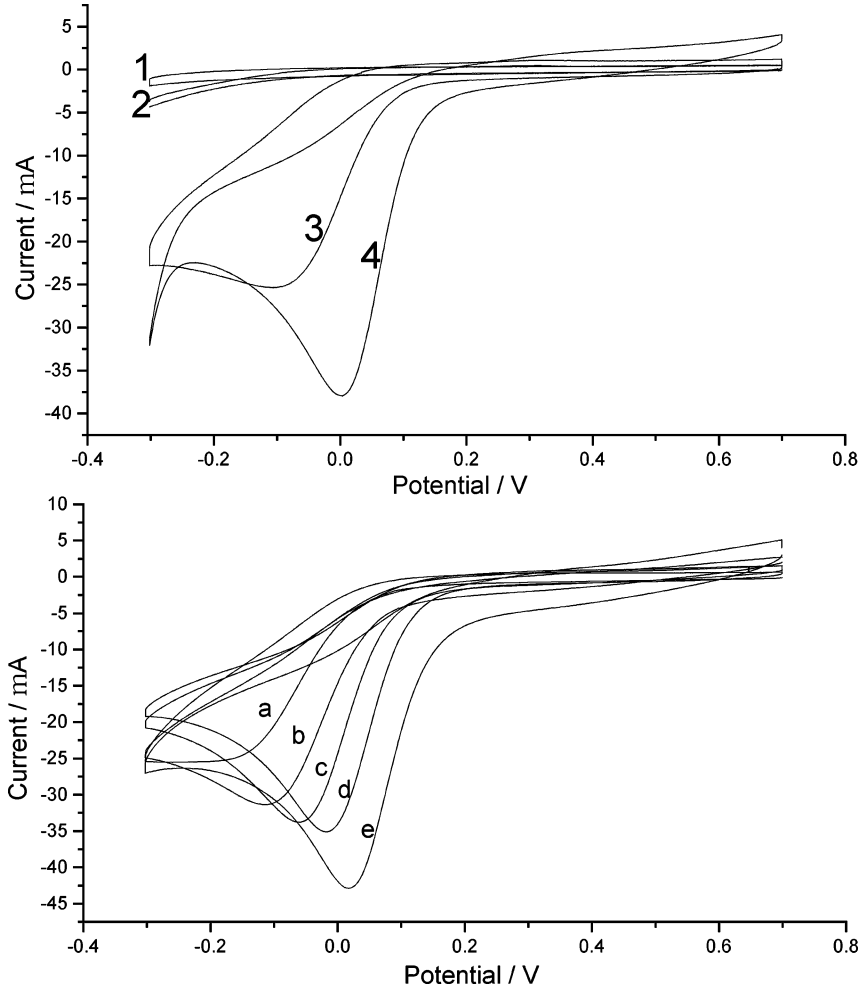

Figure 3. Cyclic voltammograms (CVs) of dioxygen reduction at 2D SANMs electrodes in air-saturated 0.1 M $HClO_4$ aqueous solution. Scan rate is 50 mV/s. Top: CVs of APTMS/ITO before (1) and after (2), and CVs of nano-gold/APTMS/ITO before (3) and after (4) immersion into 0.3 mM CoTMPyP solution for 30 min. Bottom: a, b, c, d, and e correspond to SANM electrodes with increasing number density of gold nanoparticles controlled by increasing immersion times (10, 20, 32, 95, and 180 min) in as-prepared gold colloid. All five electrodes were immersed into 0.3 mM CoTMPyP solution for 30 min before measuring CVs.

which indicates that 2D Au/CoTMPyP SANMs only reduce dioxygen to H_2O_2.

Previous studies have shown that the number density of gold nanoparticles on ITO substrate is highly tunable simply by immersion times in gold colloid.[6,8,26] Thus, the 2D SANMs can be prepared in a highly controllable way by nanoparticle self-assembly kinetics as shown in Scheme 1. The resulting materials show a tunable electrocatalytic activity toward dioxygen reduction as shown in the bottom part of Figure 3. The longer immersion times in gold colloid resulted in higher number density of gold nanoparticles.[6,8,26] The higher the number density of nanoparticles is, the larger the reduction current is and a more positive shift in cathodic peak is observed upon CoTMPyP deposition. Actually, this presents a new concept of tailoring amounts of electrocatalysts on an electrode surface by the number density of nano-gold building blocks, which is achieved in the direction parellel to the ITO surface.

Three-Dimensional Au/CoTMPyP SANMs: Three-Dimensionally Tunable Electrocatalytic Activities toward Dioxygen Reduction. The electrostatic attractive interactions between the citrate-capped Au nanoparticles and positively charged CoTMPyP are strong enough to drive the formation of 3D Au/CoTMPyP SANMs by LBL techniques. The ensembles of arranged Au nanoparticles and CoTMPyP are so-called 3D SANMs. Scheme 2 illustrates the preparative process of the 3D SANMs. The clean ITO substrate was first functionalized with APTMS and then immersed into the gold colloid to generate the first layer of Au nanoparticles. The resulting base Au nanoparticle layer was treated with an aqueous solution of CoTMPyP and the gold colloid to yield the second Au nanoparticle layer. By repeating identical steps, 3D SANMs were generated. Figure 4 shows UV−visible absorbance spectra of the 3D SANMs upon stepwise deposition of Au nanoparticle and CoTMPyP (curves 2−5 correspond to the respective Au nanoparticle layers that include top coassociated CoTMPyP). The buildup of the 3D SANMs was demonstrated by the increase in gold surface plasmon band at $\lambda = 520$ nm. The appearance of the peak around 600 nm is due to strong electromagnetic coupling among close-spaced Au nanoparticles. With increasing nanoparticle deposition, the coupling interactions become more extensive to result in the increases in peak intensity. The absorbance at $\lambda_{max} = 449$ nm is attributed to the CoTMPyP Soret band which strengthens with increasing layer number, demonstrating the increase of CoTMPyP incorporated into the 3D SANMs.

The buildup of 3D SANMs results in increasing electrocatalytic activity toward dioxygen reduction. The electrocatalytic current increases and shifts positively with the layer number as shown in Figure 5. There appears a new reduction peak at ~100 mV (versus Ag/AgCl) after the fourth Au nanoparticle layer is deposited which also shifts positively and increases in strength with increasing layer number. The two peaks indicate a two-

SCHEME 1: Schematic Illustration of Site-Selective Deposition of CoTMPyP on Gold Nanoparticle Surfaces and Tuning the Quantities of the As-Anchored Electrocatalysts by Number Density of Gold Nanoparticles[a]

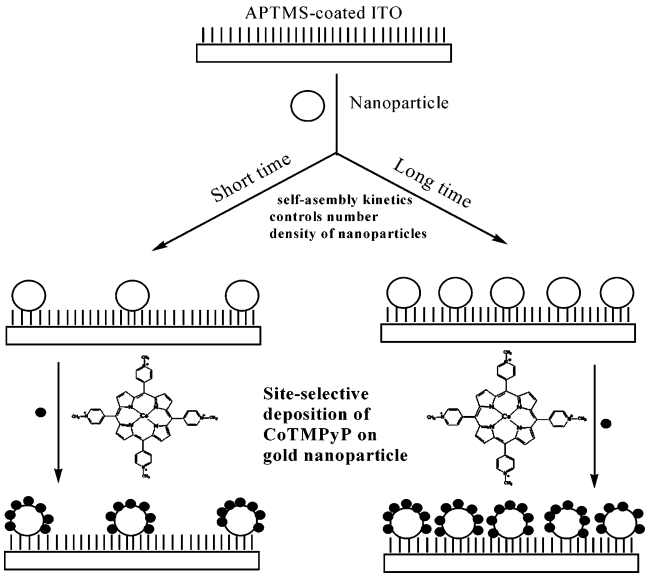

[a] The self-assembled SANMs provide a tunable electrocatalytic activity toward dioxygen reduction by controlling number density of Au nanoparticles. Inset: molecular structure of CoTMPyP.

SCHEME 2: Schematic Illustration of Preparative Process of 3D SANMs and Structure of a Mountainous Area

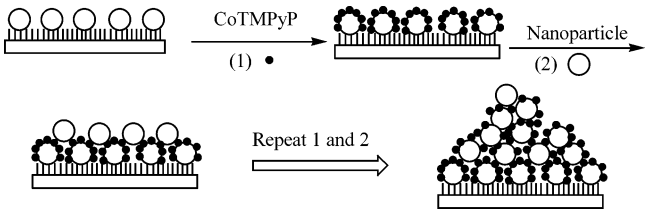

step four-electron-reduction pathway of dioxygen. A similar result[30] was also observed previously on gold nanoparticle-electrodeposited gold electrodes, which was attributed to superior activity of gold nanoparticles over bulk gold electrode.[31] Here, the two-step four-electron process might result from the domain structure of the 3D SANMs. Both the localized nanoparticle density and the close packing of CoTMPyP in the nanoparticle aggregates might affect electron transfer reactions to result in a four-electron process. Remarkably, the achieved electrocatalytic tunability is different from that achieved in the case in Figure 3. Schemes 1 and 2 illustrate clearly the different mechanisms of electrocatalytic tunability in two and three dimensions, respectively.

Film Structure and Plasmonic Properties of SANMs. Although numerous studies on LBL films of nanoparticles have been reported during the past 10 years, little investigation has been given to the fundamental structural nature of the nanoparticle films. Kotov and co-workers have used YIG nanoparticles as a model system and identified two growth modes of nanoparticle/polyelectrolyte LBL films.[32] They are normal growth mode (sequential adsorption of densely packed adsorption layers) and lateral expansion mode (in-plane growth of isolated particles). Microscopy results indicate that the origin of the lateral growth is in the interplay of particle/particle and particle/polyelectrolyte interactions rather than in a substrate

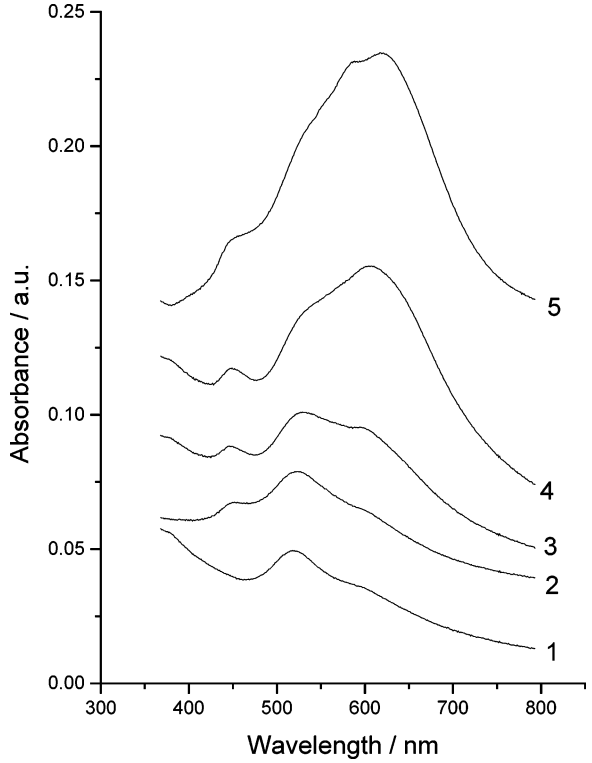

Figure 4. UV−visible absorbance spectral monitoring of growing process of ITO-supported 3D SANMs. The layer numbers are labeled beside each curve, and each curve was recorded including atop CoTMPyP layer.

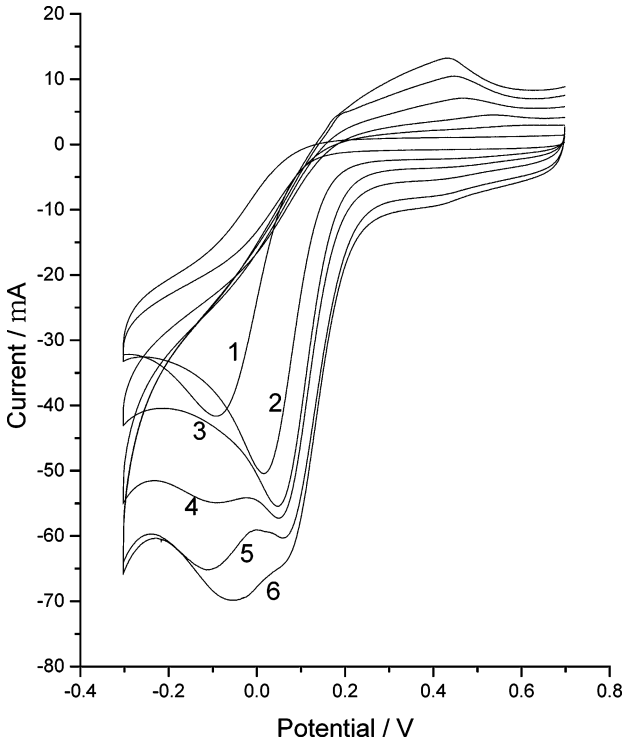

Figure 5. CVs of 3D SANMs on ITO slide in air-saturated 0.1 M $HClO_4$ aqueous solution. Scan rate is 50 mV/s. The layer numbers are labeled beside each curve.

effect. Currently, there are still no reports of the structural nature of molecular cross-linker/nanoparticle LBL films, to the best of our knowledge.

FE-SEM can be used to characterize macroscopic samples of arbitrary composition and size. The advantage of FE-SEM

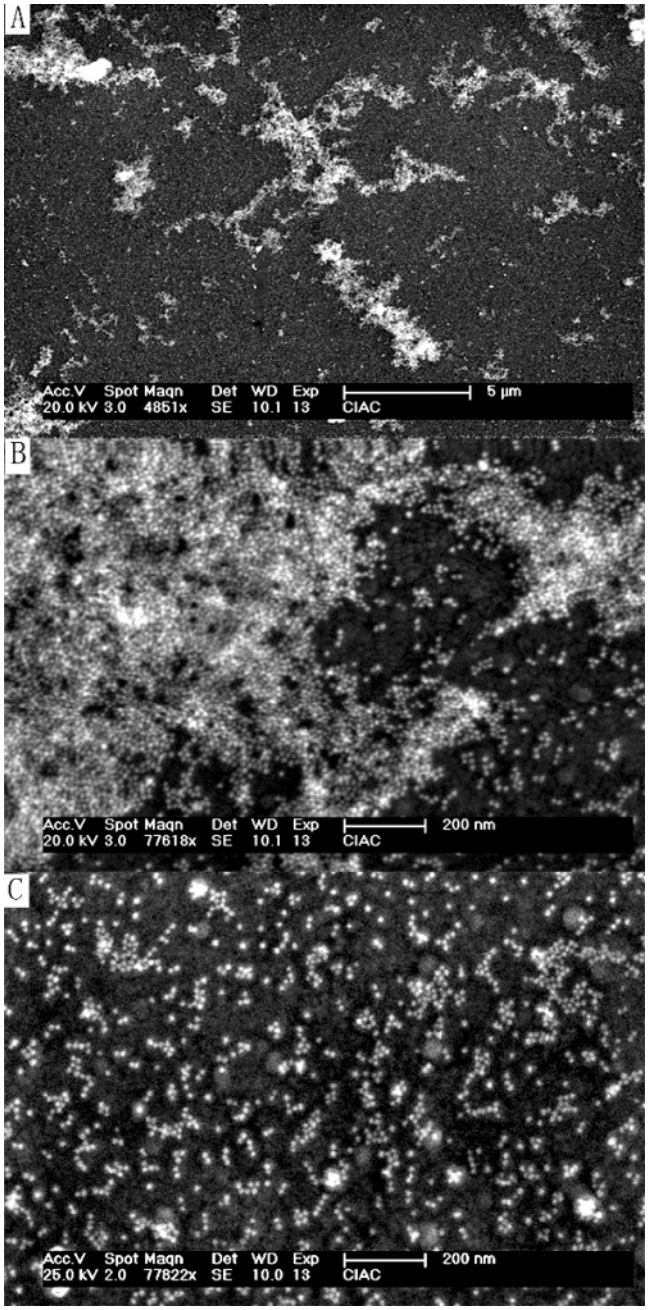

Figure 6. Typical FE-SEM images of 3D SANMs (seven Au nanoparticle/CoTMPyP layers). A, B, and C correspond to three domains at different magnifications.

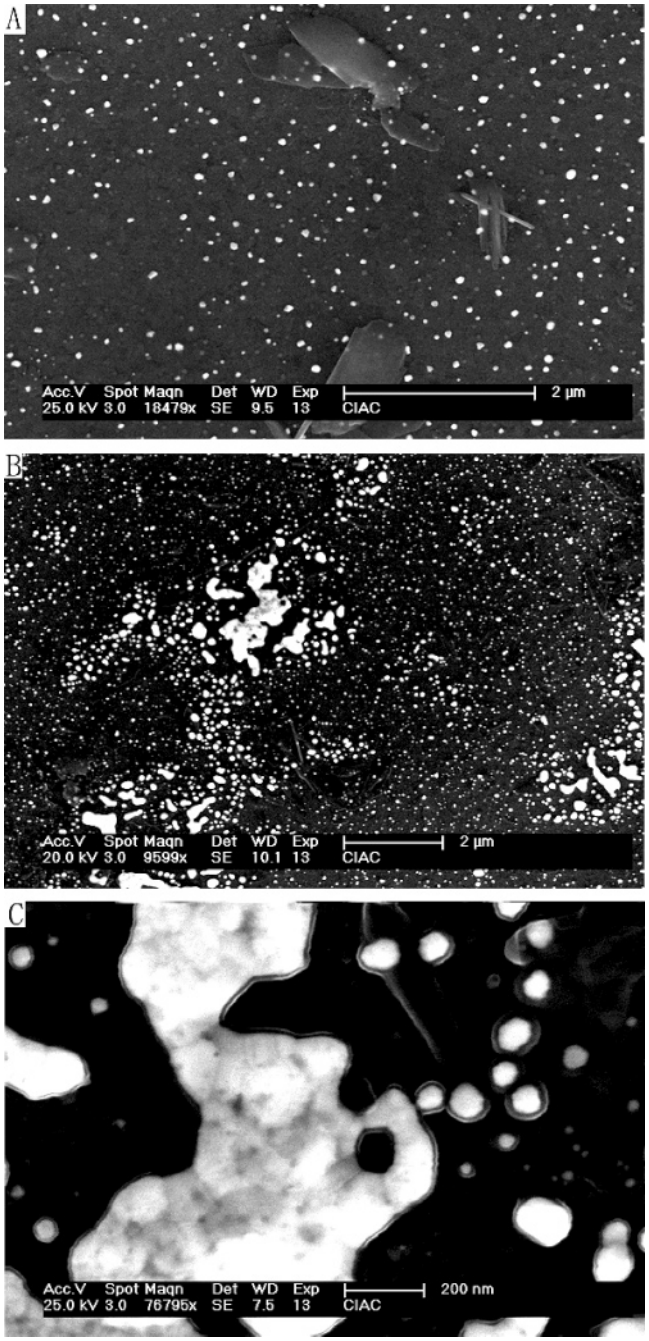

Figure 7. Typical FE-SEM images of 2D SANMs (A, one Au nanoparticle layer) and 3D SANMS (B and C, seven Au nanoparticle/CoTMPyP layers) after thermal annealing at 600 °C for 5 h.

over conventional SEM is the relatively high current density confined within a small beam, resulting in an increase in resolution. However, at such high voltages, sample charging becomes significant for nonconducting surfaces. We image directly the morphology of the 3D SANMs on conductive ITO without the use of any metallic coating, and the 3D SANM film is connected to the base copper substrates by a conductive adhesive tape. As a result, we obtain successfully the clear morphological information of 2D and 3D SANMs as shown in Figures 1 and 6.

Obviously, the as-prepared 3D SANMs grow predominantly in lateral expansion mode. Figure 6A shows clearly that the 3D SANMs are not sandwichlike with organic and inorganic strata but rather consist of irregular "huge" nanoparticle mountains and "vast" nanoparticle plains. Figure 6B shows an enlarged view of one part of a "huge" nanoparticle mountain. It is observed that the nanoparticles in the mountain are close-packed, discrete and not fuse into larger particles. Figure 6C shows an enlarged view of one part of the "vast" nanoparticle plains. The morphological characteristic of the plains is different from that of 2D SANMs (Figure 1). In the plains, there exist numerous small-scale in-plane aggregates where nanoparticles are linked by CoTMPyP and distributed in a 2D plane along the ITO surface, and only a small amount of particles are still isolated. The phenomena are consistent with poly(diallyldimethylammonium)/polystyrene mutilayers,[32] indicating the presence of the nanoparticle desorption process associated with the deposition of the CoTMPyP layers.

Furthermore, we investigate the morphological changes of 2D and 3D SANMs upon thermally annealing at 600 °C for 5 h. Figure 7 shows typical FE-SEM images of the annealed

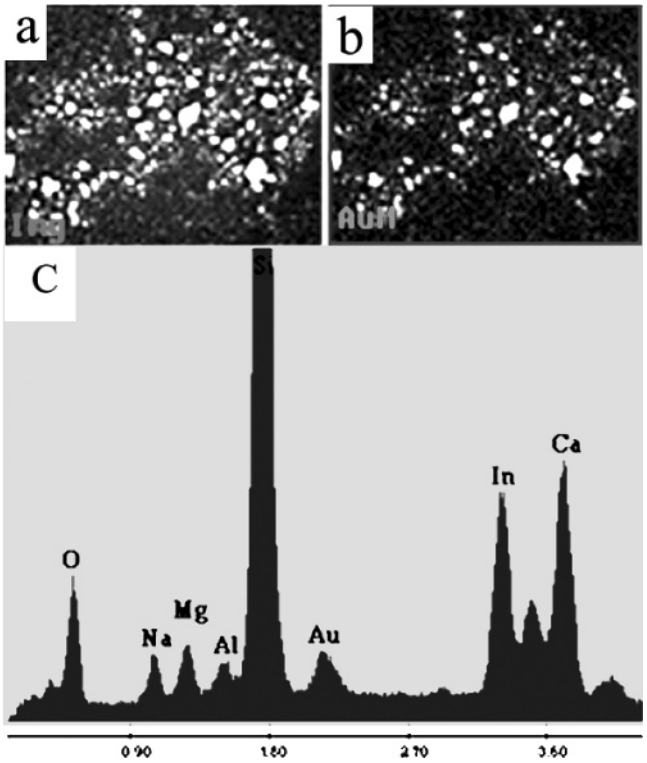

Figure 8. EDX analysis in a selected domain. Comparison of (a) (morphological image) and (b) (elemental gold map) shows that fused nanostructures are made predominantly of gold.

SANMs films. Clearly, sample morphologies are largely different from those of unannealed samples. As for 2D nanoparticlar films, particle sizes become larger and more polydisperse as shown in Figure 7A; as for 3D nanoparticlar films, it seems that Au nanoparticles in the "huge" mountains have fused into bulk gold as shown in Figure 7B,C. It has been reported recently that thermal annealing can result in atomic rearrangement in metallic nanoparticles and convert the internal particle structure from disordered phase to ordered phase.[33] Citrate ions and CoTMPyP would be burned out at 600 °C, and increasing van der Waals interactions among deprotected gold nanoparticles would result in direct contact of Au nanoparticles in the paternal nanoparticle based mountains. The atomic rearrangement would make discrete gold nanoparticles fuse into pure gold mountains. The fused mountains are predominantly made of gold as demonstrated by energy-dispersive X-ray (EDX) analysis and the corresponding elemental gold map (Figure 8). Although Au nanoparticles are well separated from each other in the 2D SANMs, they might be highly mobile at high temperature. Thus, nanoparticles could diffuse rapidly to gather in a local domain and fuse into larger nanoparticles (Figure 7A) at high temperature. Similar fast surface diffusion of ~100 nm of nanocrystals on a graphite surface was reported at even mild heating treatment.[34] XRD was used to characterize changes in the crystalline structure of the SANMs before and after annealing. As far as the (111) Bragg reflection is concerned, the (111) peak is very weak before annealing and strengthens after annealing at 600 °C for 3 h, whereas the peaks corresponding to (200), (220), and (222) are still extremely weak after annealing. This shows that annealing induced atomic rearrangement to generate predominant (111) facets.

Gold nanoparticles are especially attractive because of their strong localized surface plasmon resonance (LSPR) in the UV−visible region, which is explained as the collective oscillation of conduction electrons with incident photon frequency. The LSPR frequency is a function of size, shape, and surrounding dielectric medium. Their relationships can be expressed by eq 1,[35] where k is the absorption coefficient, N is the number density of the nanoparticles, R is the radius of the nanoparticles, ϵ_1 and ϵ_2 are the real and imaginary parts of the dielectric constants of the nanoparticles, and ϵ_m is the dielectric constant of the surrounding medium.

$$k = \frac{8\pi}{27} NR^3 \frac{\epsilon_m^{3/2} \epsilon_2}{(\epsilon_1 + 2\epsilon_m)^2 + \epsilon_2^2} \quad (1)$$

Molecular binding on the nanoparticle surface decreases the electron density of the nanoparticle surface, thereby usually dampening the intensity of LSPR band.[36]

As for the 2D gold nanoparticle arrays in this study, the gold nanoparticles are discrete from each other due to strong electrostatic repulsion.[6,8,9] Thus, the 2D gold nanoparticle arrays exhibit only one plasmon band and the increase in number density leads to the increase in LSPR peak intensity as demonstrated in previous studies.[6,8] LSPR is very sensitive to surrounding environments, and can be used as nanoscale sensor for CoTMPyP binding on gold nanoparticle surfaces as aforementioned. As for 3D self-assembled SANMs, the two plasmonic bands are observed at ~530 and ~600 nm. Although

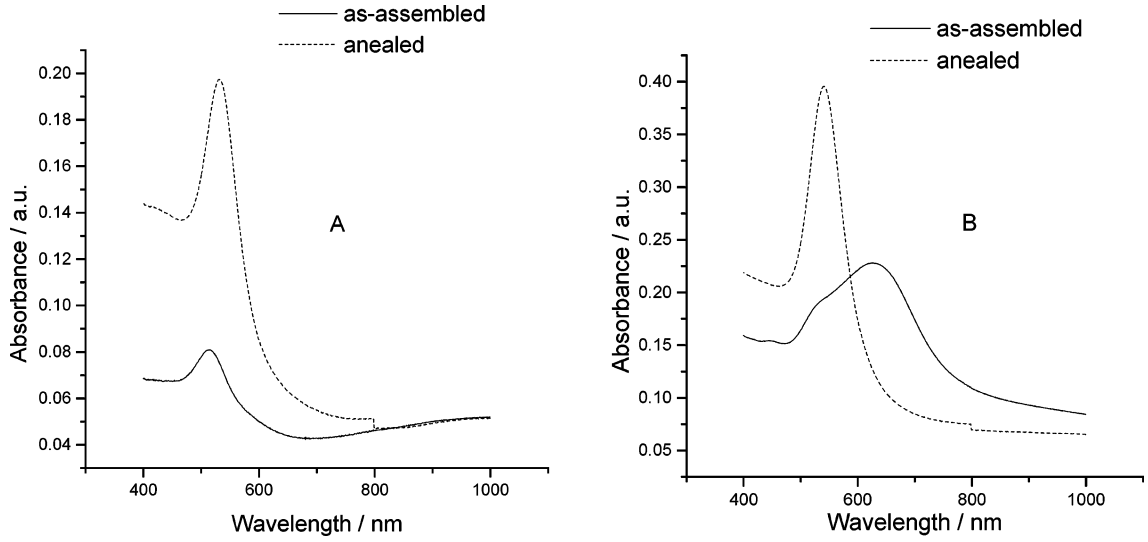

Figure 9. UV−visible spectral responses before and after annealing: (A) 2D SANMs; (B) 3D SANMs (seven Au nanoparticle/CoTMPyP layers).

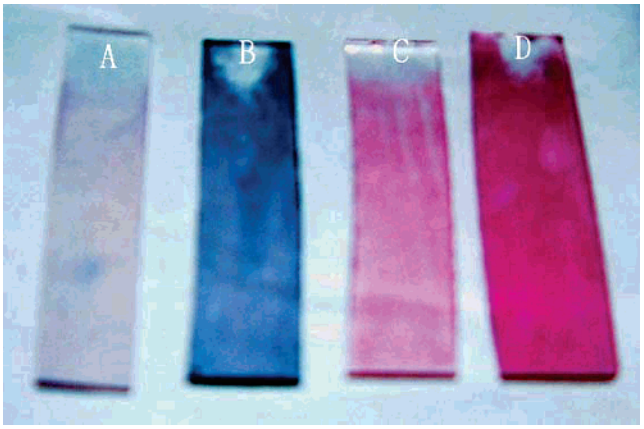

Figure 10. Photographs of 2D SANMs (A, before annealing; C, after annealing) and 3D SANMS (seven Au nanoparticle/CoTMPyP layers; B, before annealing; D, after annealing).

the similar spectral characteristic was also observed previously,[9e,11−13,17,18] little emphasis was given to the relationship between spectral responses and nanoparticle domain structure. The above FE-SEM studies have shown that 3D self-assembled SANMs are made of nanoparticle mountains and plains. The gold nanoparticles in the mountains are close-packed, and strong electromagnetic coupling[37] between close-spaced nanoparticles results in the appearance of a new absorbance band at $\lambda = \sim 600$ nm. The gold nanoparticles in the plains do not aggregate extensively and are free of strong electromagnetic coupling, which nearly keeps the native gold plasmon band at ~530 nm. The claim that the two spectral bands were caused by different nanoparticle domain structures is also supported by the following annealing experiments. The thermal annealing of both 2D and 3D SANMs results in strong enhancement in the gold surface plasmon band as shown in Figure 9. As for the 2D Au nanoparticle array, the maxium absorbance band shifts from 515 to 533 nm and the peak intensity increases ~4 times after annealing. The increase in intensity and red shift of LSPR might be due to the removal of absorbents at high temperature and size enlargement after annealing. As for the 3D SANMs, only one absorbance band at ~540 nm was observed after annealing, which seems to evolve from the disappearance of the band at longer wavelengths and the strengthening and red shift of the band at shorter wavelengths after annealing. It was thought that the former is caused by particle fusion in nanoparticle mountain domains and the latter is caused by the removal of binding molecules and particle enlargement in the nanoparticle plain domain. Figure 10 shows changes in the colors of 2D and 3D SANMs before and after annealing. As for the 2D SANMs, annealing generates a redder color because of the enhancement in LSPR intensity. As for the 3D SANMs, the stronger absorbance band is positioned in the longer wavelength region; as a result, a blue color is observed. After annealing, the color of the 3D SANMs changes to red due to the disappearance of the absorbance band.

Conclusions

Using Au nanoparticles as structural and functional units, we engineer the ITO surface to generate 2D and 3D SANMs by "bottom-up" self-assembly. The plasmonic properties and the electrocatalytic activity of the Au/CoTMPyP SANMs can be tuned by controlling parameters affecting self-assembly. These properties correlate with the structure of the SANMs. It is expected that present studies would deepen our understanding of the nanoparticle-based nanostructure−property relationship, might find application in sensors with high activity and selectivity by optimized structural design, and might also contribute to our understanding of gold nanocrystal nucleation and growth.

Acknowledgment. This work was supported by the National Science Foundation of China (No. 20275037, No. 29975028).

References and Notes

(1) (a) Frens, G. *Nature Phys. Sci.* **1973**, *241*, 20. (b) Alivisatos, A. P. *Science* **1996**, *271*, 933. (c) Landes, C. F.; Link, S.; Mohamed, M. B.; Nikoobakht, B.; El-Sayed, M. A. *Pure. Appl. Chem.* **2002**, *74*, 1675.

(2) (a) El-Sayed, M. A. *Acc. Chem. Res.* **2001**, *34*, 257. (b) Murphy, C. J.; Jana, N. R. *Adv. Mater.* **2002**, *14*, 80.

(3) (a) Kreibig, U.; Volmer, M. *Optical Properties of Metal Clusters*; Springer-Verlag: Heidelberg, Germany, 1995. (b) Olddenburg, S. J.; Averitt, R. D.; Westcott, S. L.; Halas, N. J. *Chem. Phys. Lett.* **1998**, *288*, 243. (c) Henglein, A. *Langmuir* **1999**, *15*, 6738. (d) Templeton, A. C.; Wuelfing, W. P.; Murray, R. W. *Acc. Chem. Res.* **2000**, *33*, 27. (e) Brust, M.; Walker, M.; Bethell, D.; Schiffrin, D. J.; Whyman, R. *J. Chem. Soc., Chem. Commun.* **1994**, 801. (f) Malinsky, M. D.; Kelly, K. L.; Schatz, G. C.; Van Duyne, R. P. *J. Am. Chem. Soc.* **2001**, *123*, 1471.

(4) (a) Nath, N.; Chilkoti, A. *Anal. Chem.* **2002**, *74*, 504. (b) Underwood, S.; Mulvaney, P. *Langmuir* **1994**, *10*, 3427.

(5) (a) Kalyuzhny, G.; Schneeweiss, M. A.; Shanzer, A.; Vaskevich, A.; Rubinstein, I. *J. Am. Chem. Soc.* **2001**, *123*, 3177. (b) Levlin, M.; Laakso, A.; Niemi, H. E. M.; Hautojarvi, P. *Appl. Surf. Sci.* **1997**, *115*, 31.

(6) (a) Freeman, R. G.; Grabar, K. C.; Allison, K. J.; Bright, R. M.; Davis, J. A.; Guthrie, A. P.; Hommer, M. B.; Jackson, M. A.; Smith, P. C.; Walter, D. G.; Natan, M. J. *Science* **1995**, *267*, 1629. (b) Grabar, K. C.; Freeman, R. G.; Hommer, M. B.; Natan, M. J. *Anal. Chem.* **1995**, *67*, 735.

(7) (a) Norman, S.; Anderson, T.; Granqvist, C. G.; Hunderi, O. *Phys. Rev. B* **1978**, *18*, 674. (b) Hunderi, O. *Surf. Sci.* **1980**, *96*, 1.

(8) (a) Grabar, K. C.; Smith, P. C.; Musick, M. D.; Davis, J. A.; Walter, D. G.; Jackson, M. A.; Guthrie, A. P.; Natan, M. J. *J. Am. Chem. Soc.* **1996**, *118*, 1148. (b) Musick, M. D.; Keating, C. D.; Lyon, L. A.; Botsko, S. L.; Pena, D. J.; Holliway, W. D.; McEvoy, T. M.; Richardson, J. N.; Natan, M. J. *Chem. Mater.* **2000**, *12*, 2869. (c) Patolsky, F.; Gabriel, T.; Willner, I. *J. Electroanal. Chem.* **1999**, *479*, 64.

(9) (a) Doron, A.; Katz, E.; Willner, I. *Langmuir* **1995**, *11*, 1313. (b) Cheng, W. L.; Han, X. J.; Wang, E.; Dong, S. J. *Electroanalysis* **2004**, *16*, 127. (c) Cheng, W. L.; Dong, S. J.; Wang, E. *Chem. Mater.* **2003**, *15*, 2495. (d) Park, S.; Yang, P.; Corredor, P.; Weaver, M. J. *J. Am. Chem. Soc.* **2002**, *124*, 2428. (e) Cheng, W. L.; Dong, S. J.; Wang, E. *Angew. Chem., Int. Ed.* **2003**, *42*, 449; *Angew. Chem.* **2003**, *115*, 465. (f) Menzel, H.; Mowery, M. D.; Cai, M.; Evans, C. E. *Adv. Mater.* **1999**, *11*, 131.

(10) (a) Aliev, F.; Correa-Duarte, M.; Mamedov, A.; Ostrander, J. W.; Giersig, M.; Liz-Marzan, L.; Kotov, N. A. *Adv. Mater.* **1999**, *11*, 1006. (b) Caruso, F.; Lichtenfeld, H.; Giersig, M.; Möhwald, H. *J. Am. Chem. Soc.* **1998**, *120*, 8523. (c) Caruso, F.; Caruso, R. A.; Möhwald, H. *Science* **1998**, *282*, 1111. (d) Correa-Duarte, M.; Giersig, M.; Kotov, N. A. Liz-Marzan, L. *Langmuir* **1998**, *14*, 6430. (e) Gao, M. Y.; Richter, B.; Kirstein, S.; Möhwald, H. *J. Phys. Chem. B* **1998**, *102*, 4096. (f) Liu, Y.; Wang, Y.; Claus, R. O. *Chem. Phys. Lett.* **1998**, *298*, 315. (g) Lvov, Y. M.; Rusling, J. F.; Thomsen, D. L.; Papadimitrakopoulos, F.; Kawakami, T.; Kunitake, T. *Chem. Commun.* **1998**, 1229. (h) Klwinfeld, E. R.; Ferguson, G. S. *Science* **1994**, *265*, 370. (i) Schlenoff, J. B.; Ly, H.; Li, M. *J. Am. Chem. Soc.* **1998**, *120*, 7626. (j) Mottoussi, H.; Radzilowski, L. H.; Dabbousi, B. O.; Fogg, D. E.; Schrock, R. R.; Thomas, E. L.; Rubner, M. F.; Bawendi, M. G. *J. Appl. Phys.* **1999**, *86*, 4390. (k) Ferguson, G. S.; Kleinfeld, E. R. *Adv. Mater.* **1995**, *7*, 414. (l) Kovtyukhova, N. I.; Ollivier, P. J.; Martin, B. R.; Mallouk, T. E.; Chizhik, S. A.; Buzaneva, E. V.; Gorchinskiy, A. D. *Chem. Mater.* **1999**, *11*, 771. (m) Keller, S. W.; Kim, H.-N.; Mallouk, T. E. *J. Am. Chem. Soc.* **1994**, *116*, 8817. (n) Cassagneau, T.; Fendler, J. H. *J. Phys. Chem. B* **1999**, *103*, 1789. (o) Schmitt, J.; Decher, G.; Dressick, W. J.; Brandow, S. L.; Geer, R. E.; Shashidhar, R.; Calvert, J. M. *Adv. Mater.* **1997**, *9*, 61.

(11) Shipway, A. N.; Katz, E.; Willner, I. *ChemPhysChem* **2000**, *1*, 18.

(12) (a) Lahav, M.; Heleg-Shabtai, V.; Wasserman, J.; Katz, E.; Willner, I.; Durr, H.; Hu, Y. Z.; Bossmann, S. H. *J. Am. Chem. Soc.* **2000**, *122*, 11480. (b) Lahav, M.; Gabriel, T.; Shipway, A. N.; Willner, I. *J. Am. Chem. Soc.* **1999**, *121*, 258.

(13) (a) Kharitonov, A. B.; Shipway, A. N.; Willner, I. *Anal. Chem.* **1999**, *71*, 5441. (b) Kharitonov, A. B.; Shipway, A. N.; Katz, E.; Willner, I. *Rev. Anal. Chem.* **1946**, *18*, 255.

(14) (a) Wohltjen, H.; Snow, A. W. *Anal. Chem.* **1998**, *70*, 2856. (b) Shipway, A. N.; Lahav, M.; Blonder, R.; Willner, I. *Chem. Mater.* **1999**, *11*, 13. (c) Lahav, M.; Shipway, A. N.; Willner, I. *J. Chem. Soc., Perkin Trans. 2* **1999**, 1925.

(15) McKenzie, K. J.; Marken, F. *Langmuir* **2003**, *19*, 4327.

(16) (a) Brust, M.; Etchenique, R.; Calvo, E. J.; Gordillo, G. J. *Chem. Commun.* **1996**, 1949. (b) Baum, T.; Bethell, D.; Brust, M.; Schiffrin, D. J. *Langmuir* **1999**, *15*, 866. (c) Cheng, W. L.; Dong, S. J.; Wang, E. *Langmuir* **2003**, *19*, 9434.

(17) Gittins, D. I.; Bethell, D.; Nichols, R. J.; Schiffrin, D. J. *Adv. Mater.* **1999**, *11*, 737.

(18) (a) Musick, M. D.; Keating, C. D.; Keefe, M. H.; Natan, M. J. *Chem. Mater.* **1997**, *9*, 1499. (b) Cheng, W. L.; Jiang, J. G.; Dong, S. J.; Wang, E. *Chem. Commun*. **2002**, 1706.

(19) (a) Kotov, N. A.; Dekany, I.; Fendler, J. H. *J. Phys. Chem.* **1995**, *99*, 13065. (b) Mamedov, A.; Ostrander, J.; Aliev, F.; Kotov, N. A. *Langmuir* **2000**, *16*, 3941.

(20) (a) Skandan, G. In *MRS Symposium Proceedings*; Gonsalves, K. E., Barton, M. I., Singh, R., Hofmann, H., Chen, J. X., Akkara, J. A., Eds.; Materials Research Society: Warrendale, PA, 1998; pp351−362. (b) Fan, H.; Zhou, Y.; Lopez, G. P. *Adv. Mater.* **1997**, *9*, 728. (c) Barnes, K. A.; Karim, A.; Douglas, J. F.; Nakatani, A. I.; Gruell, H.; Amis, E. J. *Macromolecules* **2000**, *33*, 4177. (d) Fritzsche, W.; Porwol, H.; Wiegand, A.; Bornmann, S.; Kohler, J. M. *Nanostruct. Mater.* **1998**, *10*, 89. (e) Chevreau, A.; Phillips, B.; Higgins, B. G.; Risbud, S. H. *J. Mater. Chem.* **1996**, *6*, 1643.

(21) (a) Kovtyukhova, N. I.; Martin, B. R.; Mbindyo, J. K. N.; Mallouk, T. E.; Cabassi, M.; Mayer, T. S. *Mater. Sci. Eng. C* **2002**, *19*, 205. (b) Crisp, M. T.; Kotov, N. A. *Nano Lett.* **2003**, *3*, 173. (c) Shi, X.; Caruso, F. *Langmuir* **2001**, *17*, 2036. (d) Caruso, F. *Adv. Mater.* **2001**, *13*, 11.

(22) Westcott, S.; Oldenburg, S.; Lee, T. R.; Halas, N. J. *Langmuir* **1998**, *14*, 5396.

(23) (a) Keller, S. W.; Johnson, S. A.; Brigham, E. S.; Yonemoto, E. H.; Mallouk, T. E. *J. Am. Chem. Soc.* **1995**, *117*, 12879. (b) Kerimo, J.; Adams, D. M.; Barbara, P. F.; Kaschak, D. M.; Mallouk, T. E. *J. Phys. Chem. B* **1998**, *102*, 9451. (c) Kotov, N. A.; Dekany, I.; Fendler, J. H. *Adv. Mater.* **1996**, *8*, 637. (d) Gao, M.; Lesser, C.; Kirstein, S. Möhwald, H.; Rogach, A. L.; Weller, H. *J. Appl. Phys.* **2000**, *87*, 2297. (e) Liu, Y.; Wang, A.; Claus, R. *J. Phys. Chem. B* **1997**, *101*, 1385. (f) Tokuhisa, H.; Hammond, P. T. *Adv. Funct. Mater.* **2003**, *13*, 831. (g) Feldheim, D. L.; Grabar, K. C.; Natan, M. J.; Mallouk, T. E. *J. Am. Chem. Soc.* **1996**, *118*, 7640.

(24) Pasternack, R. F.; Cobb, M. A. *J. Inorg. Nucl. Chem.* **1973**, *35*, 4327.

(25) (a) Shen, Y.; Liu, J. Y.; Jiang, J. G.; Liu, B. F.; Dong, S. J. *J. Phys. Chem. B* **2003**, *107*, 9744. (b) Shen, Y.; Liu, J. Y.; Wu, A. G.; Jiang, J. G.; Bi, L. H.; Liu, B. F.; Dong, S. J.; Li, Z.; Dong, S. J. *Langmuir* **2003**, *19*, 5397.

(26) Cheng, W. L.; Dong, S. J.; Wang, E. *Anal. Chem.* **2002**, *74*, 3599.

(27) (a) Malinsky, M. D.; Kelly, K. L.; Schatz, G. C.; Van Duyne, R. P. *J. Am. Chem. Soc.* **2001**, *123*, 1471. (b) Haes, A. J.; Van Duyne, R. P. *J. Am. Chem. Soc.* **2002**, *124*, 10596.

(28) Weisbecker, C. S.; Merritt, M. V.; Whitesides, G. M. *Langmuir* **1996**, *12*, 3763.

(29) (a) Kreibig, U.; Volmer, M. *Optical Properties of Metal Clusters*; Springer-Verlag: Heidelberg, Germany, 1995. (b) Eck, D.; Helm, C. A.; Wagner, N. J.; Vaynberg, K. A. *Langmuir* **2001**, *17*, 957. (c) Olddenburg, S. J.; Averitt, R. D.; Westcott, S. L.; Halas, N. J. *Chem. Phys. Lett.* **1998**, *288*, 243. (d) Henglein, A. *Langmuir* **1999**, *15*, 6738. (e) Ung, T.; Liz-Marzan, L. M.; Mulvaney, P. *J. Phys. Chem. B* **2001**, *105*, 3441. (f) Storhoff, J. J.; Lazarides, A. A.; Mucie, R. C.; Mirkin, C. A.; Letsinger, R. L.; Schatz, G. C. *J. Am. Chem. Soc.* **2000**, *122*, 4640.

(30) Nicholson, R. S.; Shain, I. *Anal. Chem.* **1964**, *36*, 706.

(31) El-Deab, M. S.; Ohsaka, T. *Electrochem. Commun.* **2002**, *4*, 288.

(32) Ostrander, J. W.; Mamedov, A. A.; Kotov, N. A. *J. Am. Chem. Soc.* **2001**, *123*, 1101.

(33) (a) Sun, S.; Murray, C. B.; Weller, D.; Folks, A.; Moser, A. *Science* **2000**, *287*, 1989. (b) Elkins, K. E.; Vedantam, T. S.; Liu, J. P.; Zeng, H.; Sun, S.; Ding, Y.; Wang, Z. L. *Nano Lett.* **2003**, *3*, 1647.

(34) (a) Ge, G.; Brus, L. E. *Nano Lett.* **2001**, *1*, 219. (b) Angelo, S. K. S.; Waraksa, C. C.; Mallouk, T. E. *Adv. Mater.* **2003**, *15*, 400.

(35) Schmitt, J.; Machtle, P.; Eck, D.; Möhwald, H.; Helm, C. A. *Langmuir* **1999**, *15*, 3256.

(36) (a) Linnert, T.; Mulvaney, P.; Henglein, A. *J. Phys. Chem.* **1993**, *97*, 679. (b) Thomas, K. G.; Zajicek, J.; Kamat, P. V. *Langmuir* **2002**, *18*, 3722.

(37) Collier, C. P.; Say Kally, R. J.; Shiang, J. J.; Henrichs, S. E.; Heath, J. R. *Science* **1997**, *277*, 1978.